UCRL-JC-127182
PREPRINT

The Effect of Jitter on an Imaging FTIR Spectrometer

C. L. Bennett

This paper was prepared for submittal to the
11th Annual International Symposium on Aerospace/Defense Sensing, Simulation and Controls
Orlando, FL
April 20-25, 1997

April 1997

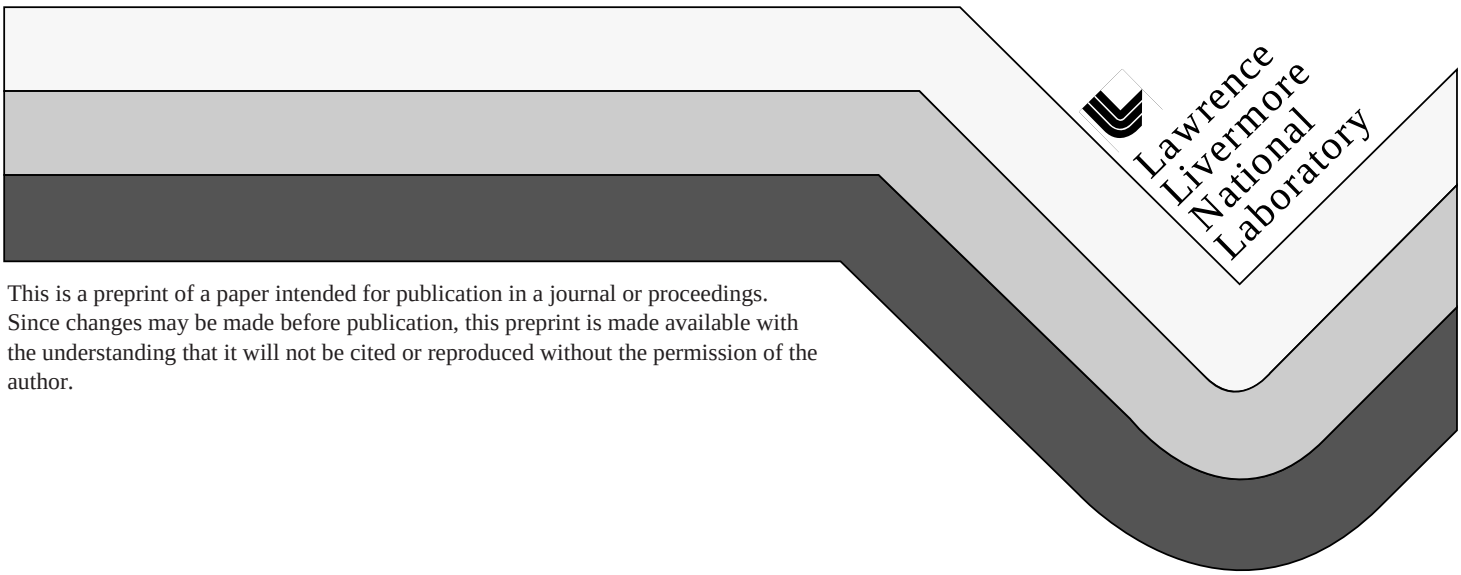

The effect of jitter on an imaging FTIR spectrometer

Charles L. Bennett

Lawrence Livermore National Laboratory, L-45, Livermore, CA. 94550

ABSTRACT

Line of sight (LOS) jitter produces temporal modulations of the signals which are detected in the focal plane of a temporally modulated imaging Fourier Transform Spectrometer. A theoretical treatment of LOS jitter effects is given, and is compared with the results of measurements with LIFTIRS[1] (the Livermore Imaging Fourier Transform InfraRed Spectrometer). The identification, isolation, quantification and removal of jitter artifacts in hyperspectral imaging data by means of principal components analysis is discussed. The theoretical distribution of eigenvalues expected from principal components analysis is used to determine the level of significance of spatially coherent instrumental artifacts in general, including jitter as a representative example. It is concluded that an imaging FTIR spectrometer is much less seriously impacted by a given LOS jitter level than a non imaging FTIR spectrometer.

Keywords: Hyperspectral Imaging, Multispectral Imaging, Imaging Spectrometer, Imaging FTIR Spectrometer, Principal Components Analysis

1. INTRODUCTION

Fourier transform spectrometers are well known to be susceptible to temporal fluctuations in the detected signal[2]. Temporal fluctuations in the detected signal may occur when the line of sight (LOS) to the observed object fluctuates and the observed object has a spatially varying radiance distribution. Frequency modulations which are within the bandpass of the modulations produced by the interferometer produce direct interference with the spectra of interest, and have been treated previously[3]. However, in addition to such "inband" frequency modulations, "outband" modulations of the LOS also produce side bands to the inband spectral features. For a non-imaging spectrometer, the modifications to the spectra produced by LOS jitter are effectively a spectral noise source, and place fairly stringent requirements on the stability of the LOS during the course of a measurement. For an imaging FTIR spectrometer, however, variations in the LOS produce changes in the spectra which are strongly correlated over the pixels in the focal plane array (FPA). In analogy to the substantial insensitivity to "common mode" electronic noise obtained by using differential signal levels, an imaging FTIR spectrometer is able to substantially reduce sensitivity to LOS jitter by use of "common mode" rejection techniques, as is described herein. Furthermore, other noise sources which have the feature that they are strongly correlated over the pixels on the FPA, may be substantially attenuated by the same method. Examples of the application of this technique to LIFTIRS (Livermore Imaging FTIR Spectrometer) hyperspectral imaging data are given.

2. FIRST ORDER MODEL

The intensity of the modulated portion of the interference pattern, in the image plane of a perfectly compensated, perfectly efficient imaging Fourier transform spectrometer is a function, $I(\mathbf{x},D)$ of the round trip optical path difference D between the two mirrors, and the position $\mathbf{x}$ in the image plane. $I(\mathbf{x},D)$, the interferogram function, is related to the Fourier transform of the detected spectral intensity $S(\mathbf{x},\nu)$, where ν is the reciprocal wavelength $1/\lambda$, or wavenumber, seen by a detector element,

$$I(\mathbf{x},D) = \int_{\nu=0}^{\infty} S(\mathbf{x},\nu)(1+\cos(2\pi D\upsilon))d\nu \quad . \tag{1}$$

Real interferometers have dispersion and are not perfectly efficient, but these complications are easily dealt with, and will be ignored in the present treatment. For a constant speed of motion of the moving mirror in the interferometer, and assuming that t=0 corresponds to 0 optical path difference, the optical path difference is given by D = v t. The interference intensity then becomes a function of time,

$$I(\mathbf{x},t) = \int_{\nu=0}^{\infty} S(\mathbf{x},\nu)(1+\cos(2\pi\nu vt))d\nu \tag{2}$$

The relation between the wavenumber ν, in units of cm^{-1}, and the modulation frequency f, in units of Hz, is given by f = ν v, where v is the rate of change of the optical path difference.

If the spectral intensity seen by a particular detector element is also explicitly a function of time, additional contributions to the interferogram function, beyond those produced by the time dependent interferometer modulation appear. If the line of sight of the imaging system is time dependent, so that the image position is a function of time, **x**= **x**(t), then the interferogram function is, in leading order, given by the expression

$$I(\mathbf{x}(t),t) = I_0(\mathbf{x}(0),t) + \nabla I_0(\mathbf{x}(0),t) \bullet [\mathbf{x}(t) - \mathbf{x}(0)] \ . \tag{3}$$

The time dependent vector **x**(t) is denoted as the jitter function. The next order term, beyond the leading order gradient expansion, is given by

$$\frac{\partial^2 I_0(\mathbf{x}(0),t)}{\partial x_i \partial x_j}[x_i(t) - x_i(0)][x_j(t) - x_j(0)] \quad , \tag{4}$$

which involves the second spatial derivatives of the un-jittered interferogram function and the second order tensor derived from products of components of the jitter function **x**(t). Higher order terms will involve corresponding higher order gradients and higher order jitter function tensors.

For a band limited spectrum, the continuous interferogram function is completely determined by a set of discrete samples. A so-called "two sided" interferogram consists of a set of N discrete samples of the interferogram function symmetric about the point t=0. For convenience in the formulas, the labeling of the discrete interferogram samples is such that $I_n = I(n\Delta t)$ (with t=nΔ, for n ε [0,N/2] and t=(n-N)Δt for n ε [N/2,N-1]). The discrete periodogram estimate, S_k , of the continuous spectral intensity S(f), is given by the discrete Fourier transform,

$$S_k = \frac{1}{N}\sum_{n=0}^{N-1} I_n \ e^{-i2\pi\frac{kn}{N}} \tag{5}$$

The discrete periodogram spectral estimate is approximately related to the continuous spectral function by $S_k = S(k\delta f)\,\delta f$, where δf is the spacing between spectral channels. The inverse transform is

$$I_n = \sum_{k=0}^{N-1} S_k \, e^{i2\pi \frac{kn}{N}} \tag{6}$$

Parseval's theorem relates the total squared magnitude of the interferogram and the spectrum by the expression

$$\frac{1}{N} \sum_{n=0}^{N-1} |\, I_n \,|^2 = \sum_{k=0}^{N-1} |\, S_k \,|^2 . \tag{7}$$

The first order perturbation to the periodogram estimate of the spectrum produced by jitter is given by the transform of expression (3), which can be written in terms of the convolution of the transforms of the two terms in the product

$$\delta S(f) = S(f) - S_0(f) = \sum_{f'} [\nabla S_0(\mathbf{x}(0), f - f') - \nabla S_0(\mathbf{x}(0), f)] \bullet X(f') , \tag{8}$$

where $S_0(f)$ is the unperturbed periodogram estimate of the spectrum in the absence of jitter, and $\mathbf{X}(f)$ is the Fourier transform of the jitter function $\mathbf{x}(t)$. The difference of terms involving f-f' and f appears in the summation because of the transform involving $\mathbf{x}(0)$ in expression (3). This can most easily be seen by considering the identity

$$\mathbf{x}(0) = \sum_{f'} \mathbf{X}(f') \ , \tag{9}$$

which follows from the definition of the Fourier transform in expression (6). The spectral error produced by a given jitter function $\mathbf{x}(t)$ is thus proportional to a convolution of the spectral content of the jitter function, given by $\mathbf{X}(f)$, with an expression involving the spatial gradient of the unperturbed spectral intensity. For an ensemble of measurements, nominally viewing the same subject, but having different line of sight functions $\mathbf{x}(t)$, an ensemble of spectral error functions are generated. In general, the phase of the jitter function $\mathbf{X}(f)$ is uncorrelated with that of the spectral gradient, and thus the mean spectral error produced by jitter is zero. The rms spectral error is non-zero, and involves the convolution of the spectral/spatial gradient term in square brackets in expression (8), and the jitter function $\mathbf{X}(f)$. It is useful to form an estimate of the level of spectral error expected in the presence of jitter, and note some of the general features of jitter generated spectral error.

3. INBAND SPECTRAL ERROR TERMS

Because of the non-zero average value of the interferogram which is produced by the "1" in the "1+cos" term in the integrand of expression (1), the spectrum $S_O(f)$ has a very large spike at f=0. This contribution to the summation in expression (8) is very important, and appears in the f'=f term. This term is dominated by the contribution given by

$$\delta S_{inband}(f) = \nabla S_0(\mathbf{x}(0),0) \bullet \mathbf{X}(f). \tag{10}$$

This term is denoted the "inband" jitter contribution to the spectral error, since jitter modulation frequencies are, in effect, directly transcribed into the spectral range of interest in the unperturbed spectrum. Using the notation that angle brackets denote ensemble averaging, for an ensemble of jitter functions one has

$$< \delta S_{inband}(f) > \; = \; < \nabla S_0(\mathbf{x}(0),0) \bullet \mathbf{X}(f) > \; = \; 0. \tag{11}$$

$$< \delta S^2_{inband}(f) > \; = \; [\frac{\partial S_0(0)}{\partial x}]^2 < \mathbf{X}^2(f) > + [\frac{\partial S_0(0)}{\partial y}]^2 < \mathbf{Y}^2(f) >. \tag{12}$$

The inband jitter error is thus directly related to the power spectrum of the jitter function.

4. OUTBAND SPECTRAL ERROR TERMS

All of the remaining contributions to the spectral error in expression (8) not included in the "inband" treatment above are denoted as "outband" jitter contributions. The outband contribution to the spectral error depends on the details of the spatial/spectral contrast factor in a much more complicated way than the inband terms. It is useful to derive some approximate expressions for this contribution. In the approximation that the jitter frequency components are uncorrelated, i.e. that

$$< X_i(f) X_j(f') > \; = \; \delta_{i,j} \delta_{f,f'} < X_i(f)^2 >, \tag{13}$$

the outband mean square spectral error is given by

$$< \delta S^2_{outband}(f) > \; = \sum_{f' \neq 0} [\nabla_x ... f' ...]^2 < X(f')^2 > + [\nabla_y ... f' ...]^2 < Y(f')^2 >, \tag{14}$$

where the terms in square brackets in expression (14) correspond to the x and y components of the term in square brackets in expression (8). In this expression, the mean square spectral error depends on a weighted sum over the jitter power spectral density. With the further approximation that the terms in square brackets are a constant fraction, C, (the "spatial/spectral" contrast factor), of the local unperturbed spectral intensity $S_0(f)$, they may be removed from the summation, leaving an expression of the form,

$$< \delta S^2_{outband}(f) > \; = \; (C \bullet S_0(f))^2 \sum_{f' \neq 0} < X(f')^2 > + < Y(f')^2 >. \qquad (15)$$

The summation over the power spectral density of the jitter function which appears in expression (15) yields the variance of the jitter function **x**(t). Thus in this approximation one has

$$\delta S_{rms}(f) = C \bullet S_0(f)) \bullet \text{std.dev.}\{\mathbf{x}(t)\} \qquad . \qquad (16)$$

This expression for the outband jitter, in contrast to the expression (12) for the inband jitter, does not depend on the details of the spectral frequency content of the jitter function **X**(f), rather, it is determined by the aggregate standard deviation of the jitter function. Also, in contrast to expression (12) for the inband jitter, for which the jitter noise to signal ratio varies across the spectrum, the outband jitter noise to signal ratio is approximately constant over the spectrum.

5. ESTIMATED CONTRIBUTIONS OF JITTER

Both the expressions for inband jitter (12), and outband jitter (16) involve products of a spatial gradient factor with a factor dependent on the magnitude of jitter. As an illustrative example of the sensitivity of the spectral noise to inband jitter, consider the following case: assume a 10% spectral radiance change per pixel of image motion, a total spectral bandpass of M=1000 spectral channels, and a 0.01 pixel amplitude of jitter motion for a particular inband frequency component f_1. This combination leads to a jitter noise term which, according to expression (12), is approximately 0.1% of the **integral** spectral radiance S_o at the frequency f_1. However, since the integral radiance extends over a range of M=1000 spectral channels, it is 1000 times more intense than the radiance within an average channel. Thus the inband jitter noise to signal ratio is approximately unity, even for such a small level of jitter! With a similar estimate for the outband jitter, namely, a spectral/spatial contrast factor, C, of 10% per pixel of image motion, and a total jitter having a standard deviation of 1 pixel, the outband jitter noise to signal ratio would be approximately 10%. Clearly the level of “jitter noise” can be quite significant, even for apparently small levels of LOS variation.

For a non-imaging FTIR spectrometer, spectral artifacts produced by jitter are indistinguishable from real spectral features, and thus LOS jitter effectively produces a stochastic noise contribution which contaminates the desired spectra. The situation is quite different for an imaging FTIR spectrometer, however, since the variations in the spectra produced by jitter are highly correlated from one pixel to the next. By using techniques analogous to common mode rejection, but generalized to multi-dimensional space, i.e. principal components analysis, it is possible to isolate artifacts produced by LOS jitter to a small dimensional subspace, and by projection, remove them, if desired.

6. PRINCIPAL COMPONENTS ANALYSIS

In order to treat the strong degree of correlation of the spectral modifications produced by LOS jitter in an imaging FTIR spectrometer, it is useful to first define various quantities. For a particular pixel of the detector in an imaging FTIR spectrometer, such as the pixel in column i and row j, a periodogram estimate of the spectrum observed at that pixel given by an expression of the form (5) is obtained. A hyperspectral datacube consists of the set of values S_{ijk}, labeled by pixel indices i,j and spectral channel k. Although the number of spectral channels implied by the name hyperspectral is not precisely defined, indeed different authors use different definitions, here hyperspectral is merely taken to mean "more than a few". The sample mean spectrum associated with a given datacube, or with a given subset of pixels within the datacube, is defined by

$$\overline{S}_k = \frac{1}{N_{pixels}} \sum_{i,j}^{N_{pixels}} S_{ijk} \ , \tag{17}$$

where the summation may be over the entire set of pixels within the datacube, or over an arbitrarily chosen subset of pixels. In either case, N_{pixels} represents the number of pixels included in the summation. The sample covariance matrix associated with a given data cube datacube, or with a given subset of pixels within the datacube, is defined by

$$C_{kk'} = \frac{1}{N_{pixels} - 1} \sum_{i,j}^{N_{pixels}} (S_{ijk} - \overline{S}_k)(S_{ijk'} - \overline{S}_{k'}), \tag{18}$$

where the normalizing factor involves N_{pixels}-1 rather than N_{pixels} in order that the sample estimate of the covariance be an unbiased estimate of the population covariance[4]. The mean spectrum, $\overline{S}$, is an M component vector, where M is the number of spectral channels in the datacube, while the covariance matrix, C is an MxM matrix.

Diagonalization of the covariance matrix (18) provides a set of M eigenvalues and eigenvectors. The eigenvectors of the covariance matrix form an orthonormal basis for the space of M spectral channels of the original datacube. By re-expressing the datacube in terms of the covariance matrix eigenvectors, a set of "eigenimages" corresponding to each of the eigenvalues of the covariance matrix may be formed. This principal components analysis[5] method, also known as factor analysis or the Karhunen-Loeve expansion[6], is quite sensitive to spectral variations correlated from pixel to pixel in the covariance matrix summation involved in expression (18).

6.1 Noise whitening

In order to precisely quantify the various modes which emerge from the principal components analysis in terms of their statistical significance it is important to normalize the datacube such that the elements, S_{ijk} , have unit expected variance, i.e. "whiten" the data. With this normalization, and in the absence of channel to channel correlations, the expectation value for the covariance matrix (18) is the unit matrix. The expectation value for the variance of the covariance matrix elements, assuming normally distributed fluctuations, is

$$\text{variance}(C_{ij}) = \frac{1}{M}(1 + \delta_{ij}(\frac{M+1}{M-1})). \tag{19}$$

For an FTIR spectrometer, the noise level for the inband spectral channels can be accurately estimated based on the behavior of the out of band noise trends. This is possible when the interferogram is sufficiently "oversampled" that there is no significant power, other than noise, outside the instrumental passband. The range of inband spectral channels is determined by the instrumental bandpass of the system, which is in turn determined by the range of sensitivity of the detector elements and the spectral range passed by a possible band limiting filter. Spectral channels outside the system bandpass acquire intensity only from instrumental noise and/or artifacts. An example of an instrumental artifact that might show up as a spurious spectral feature would be 60 Hz modulations produced by power line pickup or interference of some sort. Another example of a system artifact is that produced by detector non-linearity. Quadratic non-linearity produces spurious spectral signatures which occur at all possible sums and differences of the real spectral channels[7]. For a spectrum which extends over less than an octave, quadratic non-linearity therefore produces no inband contamination of the true spectrum.

Whitening the datacube followed by a principal components analysis is an extremely powerful technique for revealing even quite subtle instrumental artifacts. The reason for this is that many types of instrumental artifacts, other than the case of isolated bad pixels, are spread over the entire FPA, and thus contribute to the covariance matrix in a coherent way. Thus for an artifact which contributes coherently over a set of N pixels, with an rms artifact signal to system noise ratio of ε, at the single pixel level, after principal components analysis, the coherent sum over N pixels serves to "amplify" the significance of the artifact by √N, leading to a principal component signal to system noise level of √N ε. For diagnostic and evaluation purposes this amplification is very helpful in detecting artifacts. Furthermore, the spatial pattern of the eigenimages of the covariance matrix is also very helpful in identifying and characterizing the nature and source of an artifact. Such identification and quantification is useful in terms of deciding how to fix an artifact and indeed whether it is a significant enough problem that it is even necessary to fix.

In order to determine whether a given mode generated from a principal components analysis is statistically significant, it is necessary to know what the expected distribution of eigenvalues from the diagonalization of the covariance matrix should be. It is almost always found that there are only a few dominant eigenvalues emerging from the diagonalization of the covariance matrix, while most of the eigenvalues cluster around a particular "noise" floor. This feature tends to be characteristic of monochrome imagery also, and is the reason that very often substantial data compression of images[8] is possible. For most of the eigenvalues other than the few dominant ones, it is found that there is a very characteristic form for the expected distribution.

6.2 Theoretical distribution of eigenvalues of a stochastic covariance matrix

In the case that the fluctuations of the elements of the covariance matrix are independent, normally distributed, random variables, as in expression (19) above, in the limit M -> ∞, the eigenvalues of the covariance matrix follow a displaced "semi-circle" distribution. This distribution may be simply derived, (by adding one to the abscissa), from the Wigner "semi-circle" distribution[9], which is obtained for the distribution of eigenvalues of a random matrix under quite general conditions. For finite values of M, the distribution of eigenvalues from a random matrix are well approximated by the Wigner distribution, but do have some systematic differences at the edges of the semi-circle. For any specific value of M, and number of pixels N, it is easy to numerically calculate a random datacube, calculate the covariance matrix, compute the eigenvalues, and compare with the observed distribution of eigenvalues from an real datacube of the same dimensions. Such a random matrix model for the eigenvalue distribution produces a very accurate approximation to the expectation value of the eigenvalue distribution with just a single case. Deviations from the random matrix distribution are a very sensitive means to detect statistically significant deviations from a purely stochastic process, and can be used to quantitatively determine several parameters, including the number of significant principal components present in a datacube, (as well as their level of significance), the number of correlated instrumental artifacts present in a datacube, (and *their* significance), the degree of statistical independence of the spectral channels, as well as an independent determination of the underlying stochastic noise in a datacube.

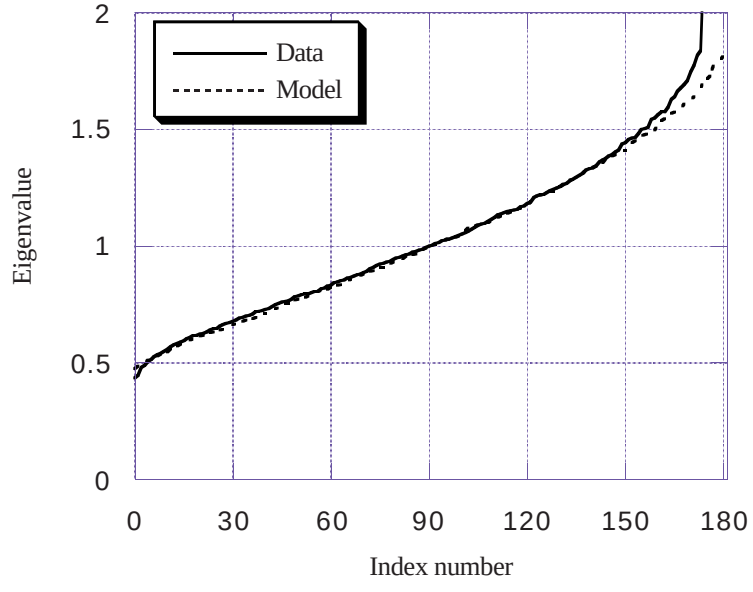

Figure 1. The distribution of eigenvalues from a random matrix model is compared with the observed distribution of eigenvalues from a hyperspectral datacube with a structured target.

As an example of the conformance of the covariance matrix eigenvalue distribution with that expected from a random matrix model, the covariance matrix eigenvalue distribution from a typical 4096 pixel subset, (corresponding to a single channel from a four channel FPA), of a LIFTIRS datacube having 181 spectral channels is compared with the eigenvalue distribution from a 4096x181 random matrix in figure 1. In this plot, the eigenvalues have been ranked in order from

the smallest to the largest. The index number indicated in the plot below corresponds to this rank ordering. As is typical of hyperspectral data, there are only a few eigenvalues which lie above the random matrix distribution, and indeed these values would plot well off the graph. The comparison shown in this figure for the lowest eigenvalues is nearly identical whether a complex scene or a flat field blackbody source is being viewed.

7. APPLICATION TO RIDGE DATA

In order to test the effects of jitter on a hyperspectral datacube from an imaging FTIR spectrometer, a 128x128 pixel, 2 cm^{-1} data cube was taken with the LIFTIRS instrument, looking at the horizon to the northwest of the laboratory. The observation of the ridge line provides a high degree of radiance contrast in the broad band image between the relatively cold sky above the horizon, and the warm hillside at the ridge. During this acquisition, the instrument was shaken vertically up and down to provide an exaggerated level of LOS jitter. From analysis of the successive images, the spatial displacement of the line of sight as a function of time was determined, and is plotted in figure 2 for the y axis (almost no jitter was present in the x direction). The rms jitter of the LOS for this data is 1.79 pixels, while the peak to peak jitter is approximately 8 pixels. By inspection of this figure, it can be seen that about 15 cycles of a nearly periodic jitter were imposed on this data.

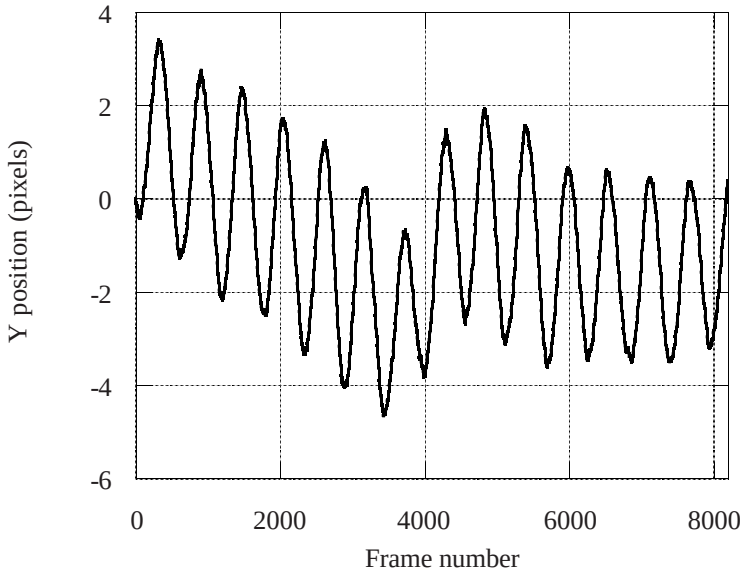

Figure 2. The relative y position of the line of sight for an artificially high level of jitter.

The image when averaged over the full acquisition period is blurred by the relatively high degree of image motion during the data acquisition. By subselection of frames taken at times for which the jitter function displayed in figure 2 deviated by less than 1/4 pixel from the initial position, and averaging over this subset, a much less blurry image may be obtained. This is illustrated in figure 3, which compares the image as averaged over all frames with the image as averaged over only the subset of nearly coincident LOS values. The amount of blurring seen in the average over all frames is common to all of the spectral channels in the hyperspectral datacube.

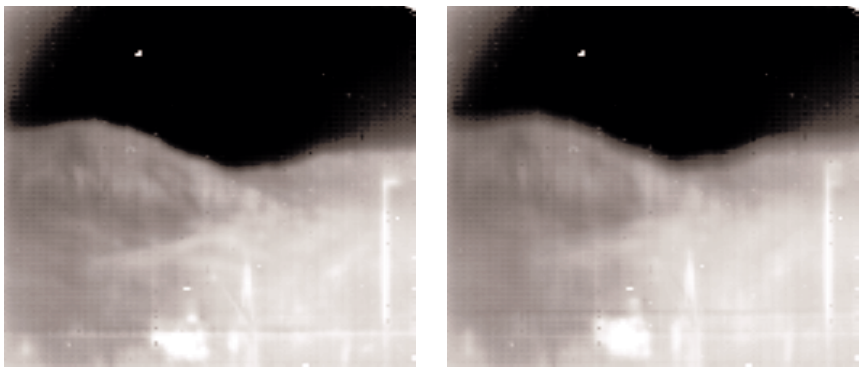

Figure 3**.** The image of the ridge line data, averaged over a subset of nearly coincident LOS positions on the left hand side is compared with the image averaged over all frames of the acquisition on the right hand side. Since the motion was primarily up and down, the blurring produced by image motion during the exposure is primarily in the vertical direction.

A typical spectrum from a pixel “on” the ridge line is compared with a typical spectrum from a pixel “off” the ridge line in figure 4. The large spikes in the spectra prominent below 10 Hz correspond to variations in the inteferogram intensity produced by the combination of a large radiance contrast at the ridge line and the large amplitude of the jitter function at low frequency. The spectral power integrated over spectral channels 13-15, which corresponds to the lowest frequency, largest amplitude spike in the power spectrum near 1 Hz, has its greatest values at the ridge line between the distant hills and

the sky, as can clearly be seen in the image displayed in figure 4. Which is simply the hyperspectral datacube "slice" corresponding to the 1 Hz frequency channel.

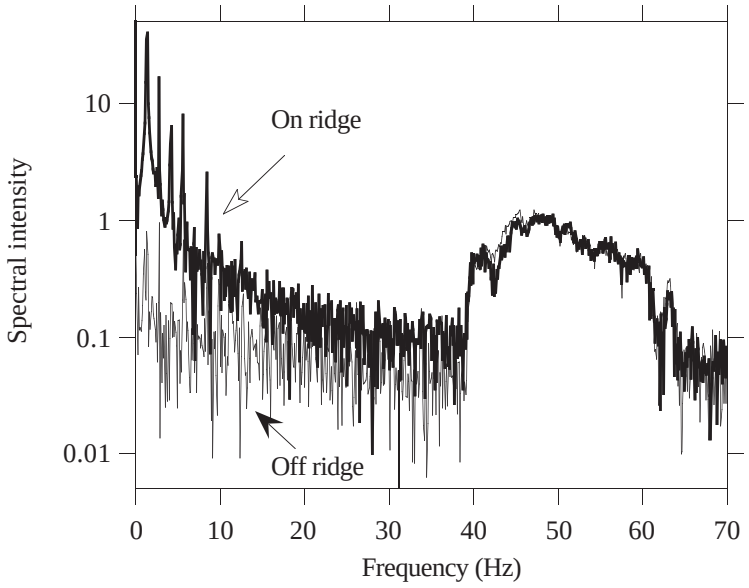

Figure 4. Spectra from pixels on and off the ridge line are compared.

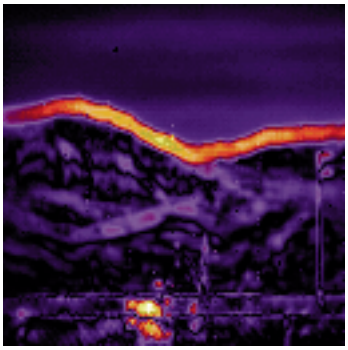

Figure 5. Image corresponding to 1 Hz channel.

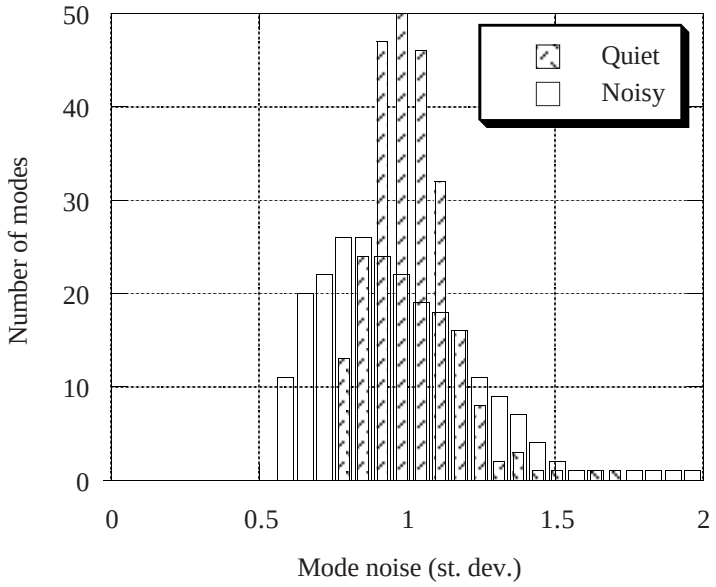

Figure 6. The eigenvalue distribution for pixels strongly affected by jitter is compared with the distribution for pixels little jitter.

Pixels in the scene were divided into two classes, based on whether the low frequency jitter power was greater or less than 20 units. There were 1775 "Noisy" pixels with more than this particular threshold level of jitter power, and 14609 "Quiet" pixels with less than this level. A principal components analysis of each of these groups of pixels was carried out, and the intrinsic hyperspectral noise level relative to the out of band estimate of the noise level was histogrammed for the eigenvalue distribution from each of the subsets. These histograms are shown in figure 6. The average noise levels were 1.039 for "Quiet" pixels, and 1.017 for "Noisy" pixels. Clearly, the level of jitter present in the ridge data produced no detectable increase in the stochastic noise level. This provides validation of the expectation that jitter noise is spatially coherent, and therefore impacts only a few principal components. It may also be seen than the distribution of eigenvalues for the 14609 pixel case approaches a Wigner semi-circle more closely than the 1775 pixel sample, as is expected for the larger statistical sample. By inspection of the larger eigenvalues produced from the principal components analysis of the jittered ridge data, it appears that for this case, only two eigenmodes are significantly elevated above the background noise level. It is plausible to identify these modes with the first order contribution of jitter expected on the basis of the leading order term shown in expression (3) above. One mode corresponds to the degree of freedom of the y direction (the stronger eigenvalue), and the other mode corresponds to the degree of freedom of the x direction (the weaker mode). Additional modes at lower levels are to be expected on the basis of higher order terms in the perturbation expansion, such as the three additional modes represented by the tensor product in expression (4). In support of the identification of particular eigenmodes as jitter modes, it is useful to examine the eigenimages produced by the principal components analysis.

The first five eigenimages from a principal components analysis of the complete set of pixels from the ridge data are shown in figure 7. A “jitter” mode is apparent in the fifth principal component, and is recognizable by the characteristic “spatial

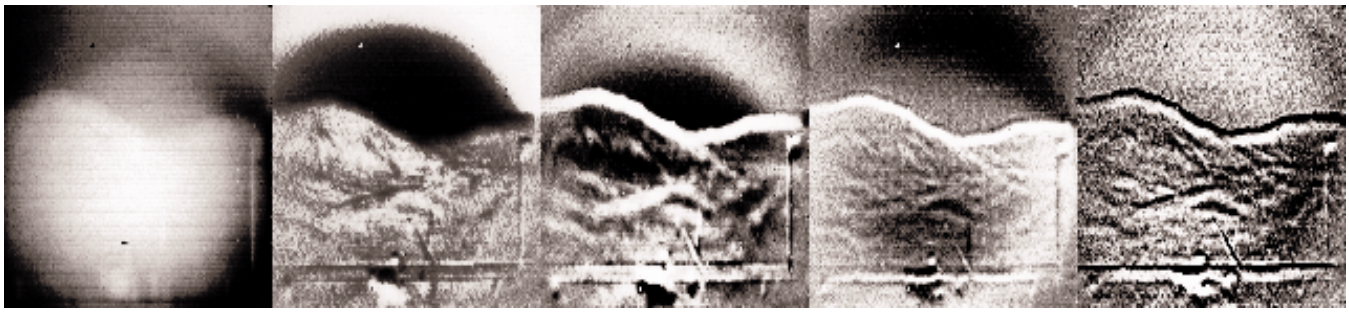

Figure 7. Eigenimages corresponding to the first five most significant eigenmodes are displayed. The eigenvalues corresponding to these images are ordered from the largest for the left hand image to the fifth largest for the right hand image.

gradient” character of the eigenimage. The fact that the jitter modes should appear proportional to the spatial gradient of the scene is to be expected on the basis of expression (8), since all terms contributing to jitter induced perturbations involve a spatial gradient of the image.

8. SUMMARY

It has been shown that the artifacts produced by line of sight jitter in the data for an imaging Fourier transform spectrometer are relatively innocuous, since they are concentrated into a relatively small number of isolated principal components. For a given level of jitter, the quantitative impact on the hyperspectral datacubes from an imaging Fourier transform spectrometer can be predicted on the basis of expressions derived in this article. It has also been shown how the significance of jitter artifacts can be placed into perspective relative to the instrumental noise level based on a principal components analysis.

ACKNOWLEDGEMENTS

This work was performed under the auspices of the U.S. Department of Energy under Contract No W-7405-Eng-48. I thank W. Aimonetti, S. Andreason, J. Bixler, M. Carter, T. Hindley, J. Marks, R. Mitchell, P. Peaslee, B. Wayne, and T. White for their help in acquiring the data that was analyzed in this article, analysis of the results, and comments on the manuscript. I thank A. Stocker and W. Kendall for discussions concerning principal component analysis.

REFERENCES

[1] C.L. Bennett, M.R. Carter, D.J. Fields, J. Hernandez, "Imaging Fourier Transform Spectrometer", SPIE Vol 1937, pp. 191-200 (1993)

2. P.R. Griffiths and J.A. deHaseth, *Fourier Transform Infrared Spectroscopy*, p. 269, John Wiley & Sons, Inc. 1986.

3. R. Beer, *Remote Sensing by Fourier Transform Spectrometry*, p. 68-69, John Wiley & Sons, Inc. 1992.

4. K. Fukunaga, *Introduction to Statistical Pattern Recognition*, p. 21, Academic Press, Inc. 1990.

5. E.R. Malinowski and D.G. Howery, *Factor Analysis in Chemistry*, John Wiley & Sons, Inc. 1980.

6. K. Fukunaga, op. cit., p. 403.

7. C.L. Bennett, M.R. Carter, D.J. Fields, “Hyperspectral Imaging in the Infrared using LIFTIRS”, SPIE Vol. 2552, pp. 274-283 (1995)

8. W.B. Pennebaker, J.L. Mitchell, *JPEG Still Image Data Compression Standard*, Van Nostrand Reinhold, New York, 1993.

9. M.L. Mehta, *Random Matrices*, p. 75, Academic Press, Inc. 1991.